Science of the Total Environment 968 (2025) 178908

Contents lists available at ScienceDirect

Science of the Total Environment

journal homepage: www.elsevier.com/locate/scitotenv

Exploring infiltration effects on coastal urban flooding: Insights from nuisance to extreme events using 2D/1D hydrodynamic modeling and crowdsourced flood reports

Sergio A. Barbosa [a,*], Yidi Wang [a], Jonathan L. Goodall [a,b]

[a] *Dept. of Civil and Environmental Engineering, University of Virginia, Charlottesville, VA 22904, USA*
[b] *Link Lab, School of Engineering and Applied Science, University of Virginia, Charlottesville, VA 22904, USA*

HIGHLIGHTS

- Pluvial flooding in an urban coastal watershed was simulated using a 1D/2D model.
- Crowdsourced flood reports of street flooding were used to evaluate the model.
- Adding infiltration in the model reduces flood extent by 33 % for nuisance flooding.
- For extreme events, flood extent decreases by 5 % including infiltration.
- The results show that infiltration is important for nuisance flood modeling.

GRAPHICAL ABSTRACT

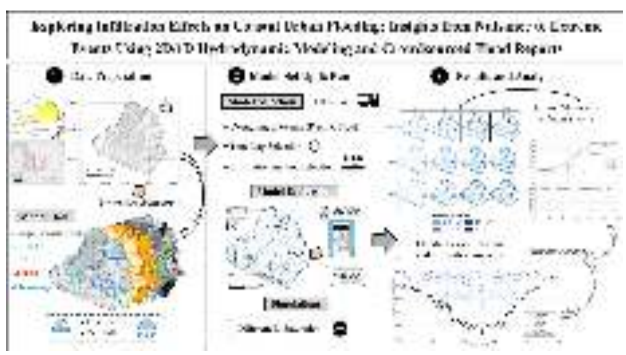

ARTICLE INFO

Editor: Elena Paoletti

Keywords:
Coastal flooding
Nuisance flooding
Extreme flooding
Infiltration losses
Hydrodynamic modeling
Crowdsourced flood report

ABSTRACT

Coastal urban flooding presents significant challenges due to the complex interactions between surface runoff, storm tides, and drainage systems. In highly impervious urban areas, infiltration may seem negligible, particularly during extreme events when soil saturation is rapidly exceeded. However, for nuisance flooding—becoming more frequent due to sea level rise and shifting rainfall patterns—the role of infiltration warrants closer examination. This study aims to assess the impact of incorporating infiltration processes into an urban flood model by evaluating flood extent under 1-, 10-, 50-, and 100-years return periods. Specifically, we performed our test case over an urban coastal watershed in Norfolk, Virginia using a detailed 2D/1D hydrodynamic model. For the evaluation of the model, we incorporated community-sourced inputs from residents and drivers collected through data portal application and a mobile navigation platform. The results show that infiltration losses reduced the flooded areas by 33 % during the 1-year return period and by 12 %, 9 %, and 5 % during 10-, 50-, and 100-years return periods respectively. In terms of flood volume, infiltration led to a 29 % reduction for the 1-year event, while reductions were smaller for extreme events due to rapid soil saturation. We also found significant variability in water depth, with for example a nearly 20 cm difference between full and zero saturation conditions during the nuisance flooding event on a selected street in the Park Place neighborhood. While less intense nuisance storms did not achieve full soil saturation, thereby reducing flood impacts, extreme events

* Corresponding author.
E-mail addresses: rqt5kh@virginia.edu (S.A. Barbosa), yw5vq@virginia.edu (Y. Wang), goodall@virginia.edu (J.L. Goodall).

https://doi.org/10.1016/j.scitotenv.2025.178908
Received 11 October 2024; Received in revised form 13 February 2025; Accepted 17 February 2025
Available online 22 February 2025

rapidly overwhelmed infiltration capacity, leading to increased surface runoff and flood inundation. Finally, the study showed how crowdsourced flood reports can help to validate urban flood models. In our case, the model accurately predicted flood locations with 88 % of community reports and 89 % of driver reports of flooding aligning with simulated inundation maps.

1. Introduction

Urban flooding poses significant challenges to both individuals and communities, particularly in terms of economic impacts (Vu et al., 2024). These include property damage, wage losses for those unable to commute, increased travel times due to rerouted traffic, disruptions in supply chains at various levels, school closures affecting parents, sudden power outages, communication breakdowns, and the contamination of water sources leading to the spread of waterborne diseases and threats to public health (Mahmood et al., 2017; E P A, 2018; Walsh et al., 2016; Brown and Murray, 2013; Hoang and Fenner, 2016; Tunstall et al., 2006; Curriero et al., 2001; Weber, 2019; Zandsalimi et al., 2024). This trend is attributed to a combination of factors including extreme weather events, rapid urbanization, and climate change, resulting in increased severity and frequency, thereby posing heightened risks to human well-being, infrastructure, and the environment (Agbola et al., 2012; Huong and Pathirana, 2013; Mahmood et al., 2017; Mahmoud and Gan, 2018; Ntelekos et al., 2010; Teng et al., 2017).

Climate change further complicates the challenges of urban flooding by significantly altering hydrological processes. It intensifies extreme rainfall events, heightening flood risks, while simultaneously increasing temperatures and evaporation rates (Tran et al., 2024), leading to drier antecedent soil moisture conditions. This combined effect creates a complex interplay of opposing forces. Studies indicate that a warmer atmosphere retains more water vapor, increasing the intensity of rainfall and heightened runoff potential (Tyndall Centre, 2021). However, higher evaporation rates also dry out soils, reducing their ability to absorb water and increasing flood vulnerabilities in some regions (C2ES, 2023). These dynamics are further influenced by spatial and temporal variations in water availability, with regions transitioning from dry to wet climates experiencing distinct shifts in flood patterns (Tabari, 2020). Understanding these intricate interactions is critical for developing robust flood risk models and implementing effective adaptation strategies to address the multifaceted impacts of climate change on urban flooding.

In coastal cities, flooding primarily results from two key processes: tidal flooding caused by extreme high tides and surface runoff resulting from heavy rainfall (Archetti et al., 2011; Dawson et al., 2008; Wahl et al., 2015; Xu et al., 2014). In certain urban areas with deficient or inadequate storm drainage systems, flooding can occur due to the excessive runoff generated by heavy rainfall, highlighting the need for accurate urban flood prediction to address these significant challenges (Fernández and Lutz, 2010; Upadhyaya et al., 2014; Wang et al., 2019; Weber, 2019; Yazdanfar and Sharma, 2015). In a typical urban environment, stormwater collected by drainage systems is typically discharged into the ocean through gravity-fed channels or pumping mechanisms. However, during periods of exceptionally high tides, the capacity of these drainage systems is significantly reduced, leading to the possibility of reverse flow and exacerbating flooding issues. The generated runoff travels across the surface, accumulating in low-lying areas within the catchment until it eventually drains, infiltrates, or evaporates (Huong and Pathirana, 2013; Mahmoud and Gan, 2018; Villarini et al., 2011).

To better understand the varying impacts of urban flooding, events can be categorized by their probabilities of exceedance (National Weather Service, 2012). Floods are typically classified into three categories: (1) extreme floods (with a probability of exceedance <5 %) characterized by severe property damage, structural failures, and high risks of injury and fatalities; (2) major floods (with a probability of exceedance between 5 % and 50 %) that can lead to substantial infrastructure damage and potentially result in loss of life; and (3) minor floods (with a probability of exceedance >50 %, also referred to as nuisance flooding) that tend to have a relatively limited impact on the public (National Weather Service, 2012). Moftakhari et al. (2018) describe nuisance flooding as "low-level inundation" that, while not posing significant threats to public safety or causing major property damage, occurs relatively frequently. These events are typically small in magnitude and are associated with short return periods, such as annual or even monthly occurrences.

Efforts to model the combined impacts of storm tide and rainfall across these various intensity events have led to the development of several methodologies. Previous studies have primarily focused on integrating a one-dimensional (1D) or two-dimensional (2D) overland model with a 2D or three-dimensional (3D) storm surge model. Software such as ADCIRC, HEC-RAS, MIKE21, and Delft3D, are commonly used to capture the interactions between storm tide and rainfall, providing comprehensive insights into flood mechanisms (Bacopoulos et al., 2017; Karamouz et al., 2017; Ray et al., 2011; Silva-Araya et al., 2018; Tahvildari et al., 2022; Yin et al., 2016b; Yin et al., 2016a). For instance, Yin et al. (2016a) introduced a coastal inundation model by integrating a storm surge model (ADCIRC) with an urban flood model (FloodMap). This coupled model, when applied at the city scale, exhibited enhanced performance compared to standalone ADCIRC modeling, notably in flood extent and depth. Similarly, Silva-Araya et al. (2018) coupled a 2D hydrologic model with a 2D storm surge model for Puerto Rico. In this approach, the storm surge model operated first to establish a tidal boundary for the hydrologic model. The findings revealed that the interaction between pluvial flooding and tidal flooding led to increased flood levels compared to storm surge alone. Ray et al. (2011) investigated how storm surge and inland rainfall jointly affect the floodplain of a coastal bayou in the Houston area. By employing dynamic hydraulic modeling, they evaluated the additional impact of storm surge on traditional rainfall-based floodplain assessments. Using data from Hurricane Ike, the study underscored the importance of considering both the timing and interaction of rainfall and storm surge in understanding inland flooding dynamic. Tahvildari et al. (2022) integrated storm surge and rainfall-driven flood models using the Delft3D-FLOW hydrodynamic model to assess roadway inundation during hurricanes. They optimized ambulance positioning to ensure critical trauma center access within the "golden hour." Applied to Hurricane Irene (2011), their framework accurately predicted flood extents and identified inadequate ambulance coverage. Adding stations improved trauma center access for most traffic zones, providing valuable insights for emergency planning in flood-prone coastal regions.

Another important component of flood modeling is the integration of one-dimensional (1D) pipe flow with two-dimensional (2D) overland flow to better capture the dynamics of urban flooding. While subsurface drainage systems are essential for managing floodwaters in urban areas, they are often omitted from coastal flood models due to data limitations. However, incorporating both 1D and 2D flow components greatly enhances the accuracy of flood simulations and is a well-established approach for assessing urban flood risks (Fan et al., 2017; Leandro et al., 2009; Martins et al., 2016; Russo et al., 2015; Seyoum et al., 2012; Yan et al., 2024). Software capable of simulating both 1D drainage network hydrodynamics and 2D surface flow, such as InfoWorks ICM, CADDIES, MIKE 21, and TUFLOW (used in this study), are widely recognized for urban inundation modeling (Mignot and Dewals, 2022; Tan et al., 2024; Wang et al., 2021; Wu et al., 2017; Ye et al., 2022). In urban coastal watersheds, studies employing 1D/2D modeling approaches to simulate overland and stormwater drainage flow have proven the effectiveness of this approach. For example, Shen et al. (2019) assessed flood risk in Norfolk, VA, by integrating historical data with hydrodynamic modeling to evaluate the combined effects of storm tide and heavy rainfall. Expanding on this, Shen et al. (2022) focused on future scenarios, highlighting that tidal flooding is expected to become dominant by 2070 due to sea level rise.

Despite the integration of multi-dimensional hydrodynamic models for urban flooding, the role of infiltration is often overlooked. This oversight stems from the generally lower infiltration rates in these environments compared to natural settings, primarily due to the prevalence of impervious surfaces (Huong and Pathirana, 2013; Mahmoud and Gan, 2018; Villarini et al., 2011). Consequently, many models assume minimal impact of infiltration during extreme storms due to these impervious surfaces (Huong and Pathirana, 2013; Mahmoud and Gan, 2018; Villarini et al., 2011; Shen et al., 2019). However, while this assumption may be held under fully saturated conditions of the soil, it does not completely capture the complexities of urban flood dynamics across different levels of soil saturation. For instance, Hossain Anni et al. (2020) utilized a 2D hydrodynamic model (MIKE URBAN) to simulate flood events on the University of Alabama, considering different storm events (10-, 25-, 50-, and 100- years return period). Their study demonstrated that variations in infiltration rates and soil moisture directly impact flood behavior, highlighting the sensitivity of flood predictions to both the value and distribution of soil inputs.

This study aims to assess the role of infiltration in coastal urban flood modeling by evaluating its impact across various storm return periods, with a focus on how infiltration varies with storm size. We quantify the effects of infiltration during nuisance, major, and extreme storm events using the Green-Ampt (GA) method, which simulates infiltration based on soil hydraulic properties. This process is integrated into a hydrodynamic model that combines 2D surface flow and 1D pipe network simulations. The model evaluates the combined effects of storm tide and rainfall across different return periods, focusing on Norfolk, Virginia's Park Place neighborhood during a nuisance flooding event. Validation was conducted using community flood reports from residents, city staff, and drivers, ensuring the model reflects real-world conditions.

The novelty of this study lies in the systematic assessment of infiltration across multiple storm scenarios and return periods, offering valuable insights for improving flood resilience in coastal cities. This approach enhances the understanding of the relationship between storm size, infiltration, and urban flooding, supporting more effective flood mitigation and disaster preparedness strategies in similar coastal communities. Specifically, we hypothesize that the inclusion of infiltration processes in urban flood models significantly reduces the extent and volume of flooding during nuisance events (e.g., 1-year return period), but its impact diminishes as storm intensity increases because of the limited storage capacity of soil storage within urbanized environments. Additionally, variations in soil saturation levels strongly influence urban flood dynamics, with lower saturation levels leading to greater infiltration potential and reduced surface runoff. Furthermore, we hypothesize that crowdsourced flood reports enhance the accuracy of hydrodynamic flood models, improving their ability to predict flood-prone areas and validate simulated flood extents. These hypotheses will be tested using a 2D/1D hydrodynamic model incorporating infiltration processes, applied to coastal urban flooding scenarios, and validated against community-sourced flood data.

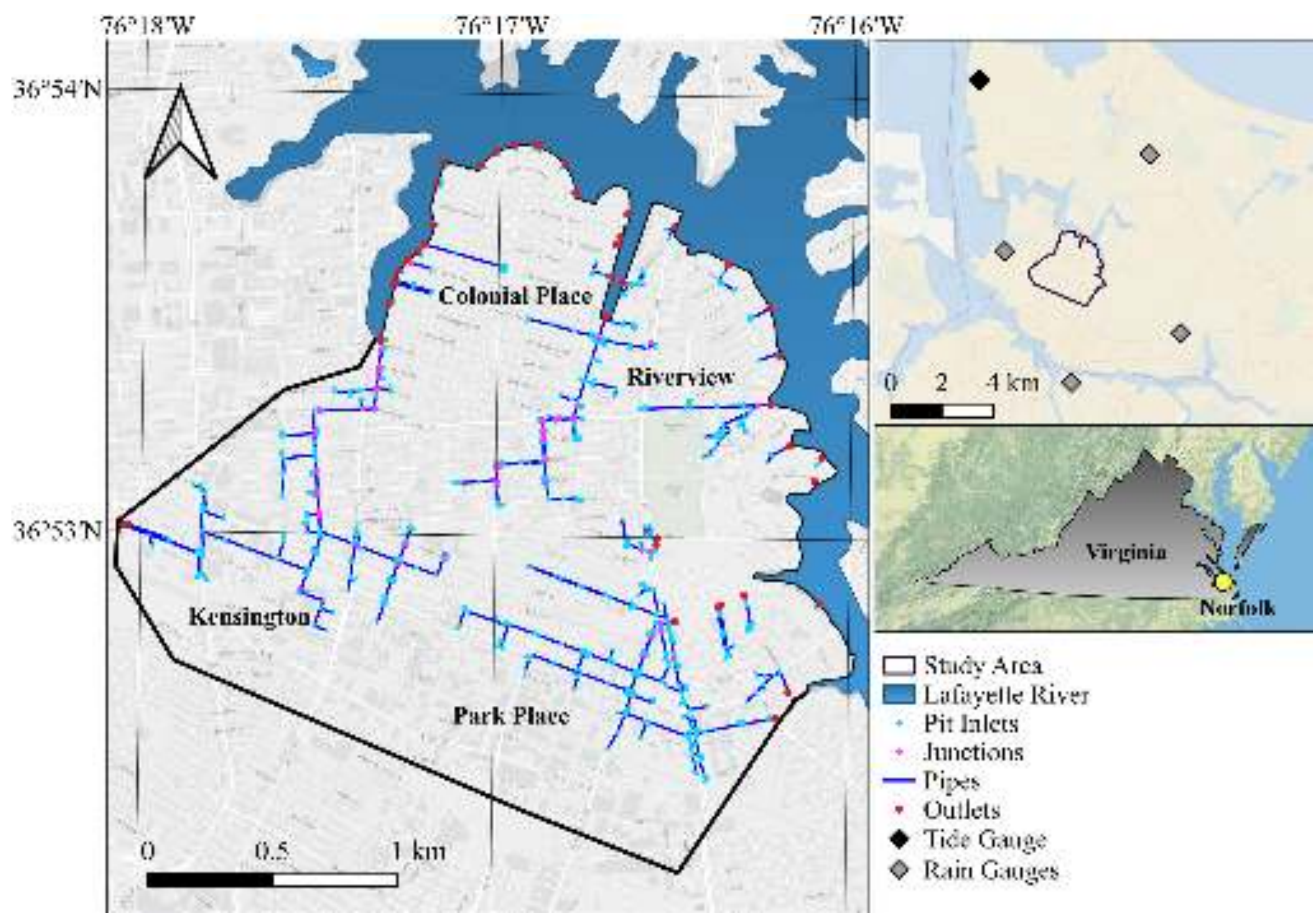

Fig. 1. Study area highlighting the locations of tide gauges, rain gauges, and the drainage system.

2. Methodology

2.1. Study area

The study area is situated in the heart of Norfolk, Virginia, USA (Fig. 1). Norfolk is a densely urbanized area characterized by predominantly flat terrain, with nearly all regions lying below an elevation of 4.5 m (North American Vertical Datum of 1988: NADV 88). This low elevation, coupled with tidal connections to the Chesapeake Bay, exposes a substantial portion of the city to the risk of tidal flooding. This risk is further exacerbated by the looming threats of sea level rise and land subsidence, as highlighted in studies by (Li et al., 2013; Sadler et al., 2017). The study domain is bounded to the north by the Lafayette River, encompassing a total area of 5.08 km^2 including four neighborhoods (Colonial Place, Riverview, Park Place and Kensington). Within this area, 2.95 km^2 consists of built-up areas, and 2.13 km^2 comprises natural terrain. Ground surface elevation within the study domain ranges from approximately −2 m to 6 m. Notably, there are no hydraulic structures, such as flood walls or tide gauges, situated between the domain outfall and the Lafayette River.

In this study, tide level data was gathered from the Sewells Point station (Station ID: 8638610), situated approximately 7 km from the tidal boundary of the domain (Fig. 1). This tide gauge has the longest tide level record in Virginia, spanning back to 1927. On the other hand, rainfall data were sourced from the National Oceanic and Atmospheric Administration (NOAA Atlas 14) and integrated into the model using four weather stations operated by the Hampton Roads Sanitation District (HRSD). On average, these HRSD stations are located around 4.2 km from the center of the study domain.

2.2. Methods

Supplementary Figure SF1 illustrates the framework used in this study to evaluate the impact of infiltration on coastal urban flooding, with a focus on distinguishing nuisance floods from major and extreme events. The approach integrates key components, including hydrological data (rainfall and tide levels), drainage network data, and spatial data such as Digital Elevation Models (DEM), land cover, soil types, and imperviousness of surface.

To set up the model, we designed scenarios that simulated combined flood events driven by both storm tides and rainfall. These scenarios aimed to capture a range of flood conditions, from nuisance to extreme events. To enhance model accuracy, we integrated community-sourced flood reports from Norfolk. Infiltration losses were estimated using the GA method, which was incorporated into the model to represent soil absorption and its influence on flood dynamics.

After running the simulations, we evaluated the impact of varying soil saturation levels on flood extent and intensity across events corresponding to four defined return periods. The analysis then shifted to examining the infiltration dynamics specifically associated with nuisance flooding events, as infiltration tends to play a more significant role in these more frequent, lower-intensity floods.

2.3. Data

To ensure a thorough evaluation of infiltration's role in coastal urban flooding, we utilized a detailed dataset incorporating multiple data sources. This dataset provides a comprehensive representation of the study area and its hydrological characteristics. The types of data used in the study include:

2.3.1. Digital elevation model (DEM)

The model's domain boundaries and topography were established using a 1m×1m Lidar DEM obtained from the Virginia Geographic Information Network (VGIN) (Supplementary Figure SF2A). This approach ensures a comprehensive understanding of the terrain within the study area. Particularly, our analysis excludes any rainfall-induced flow originating from adjacent watersheds, whether through surface runoff or pipe networks, simplifying the model for focused investigation.

2.3.2. Imperviousness

This parameter is essential because it influences the amount of water that can infiltrate into the ground by altering the soil infiltration rate (TUFLOW manual, 2018). The imperviousness with spatial resolution of 30 m was obtained from the National Land Cover Dataset (Supplementary Figure SF2B). In this study, we associated the impervious values with four different land cover types, considering their spatial distribution. We selected the highest imperviousness value for each land cover type to represent the worst-case scenario for infiltration capacity (Supplementary Table ST1).

2.3.3. Land cover

A land cover dataset with 1-m spatial resolution, retrieved from the VGIN was used to delineate overland roughness, building outlines, and road centerlines (Supplementary Figure SF2C). The Manning's roughness coefficients for overland flow, sourced from McCuen (1998), were then allocated to the 2D domain based on the corresponding land cover types, as illustrated in Supplementary Table ST2.

2.3.4. Soil type

We obtained soil type data for the study area (Supplementary Figure SF2D) from the U.S. Department of Agriculture (USDA). The area is predominantly covered by Sandy Loam, with smaller areas of Silty Clay Loam and Silt Loam. Soil properties such as suction value, hydraulic conductivity, and porosity were defined according to TUFLOW specifications.

2.3.5. Drainage system

The drainage system utilized in our study was derived from the TUFLOW model developed by Shen et al. (2022) in Norfolk. It includes three key components: inlets, pipes, and outlets. In TUFLOW, inlets are modeled as pits, where depth-discharge relationships control the stormwater flow rate entering the drainage system, depending on the type and dimensions of the inlets. The system comprises 9087 pipe sections totaling approximately 222 km in length obtained from Norfolk City. To enhance the model's efficiency and accuracy, pipes with diameters smaller than 15 in., as well as those situated within buildings, underpasses, and tunnels, were excluded from consideration (Fig. 1). Detailed information on the drainage system can be found in Shen et al. (2022).

We extracted the drainage system from the four specified neighborhoods, encompassing 841 pipe sections with a total length of 21.7 km. Additionally, we incorporated 51 junctions at critical intersections within the drainage system to improve the representation of flow dynamics. This addition was essential for accurately simulating the distribution and convergence of flow, preventing errors in the representation of inlets at these points. This aspect of our analysis was crucial for optimizing the model's representation of urban hydrology.

Supplementary Table ST3 presents the datasets utilized for constructing the urban flood model, providing insight into the various types of data integrated into the modeling process.

2.4. Urban flood simulation and model configuration with TUFLOW

The hydrodynamic TUFLOW (Two-dimensional Unsteady FLOW) model was designed specifically to simulate depth-averaged, one- and two-dimensional free-surface flows. Originating from a collaborative research and development effort funded by WBM Pty Ltd. and The University of Queensland, its primary objective was to establish a 2D modeling system with dynamic connections to a 1D system (Syme, 2001). This model effectively addresses the full set of 2D depth-averaged momentum and continuity equations governing shallow water free surface flow. Furthermore, it incorporates the extensive capabilities of the ESTRY one-dimensional (1D) hydrodynamic network, as outlined by Syme (2001).

Given the densely urbanized nature of the research area, characterized by complex flow patterns and pathways, flood modeling becomes particularly challenging due to the interaction between 2D surface flow and 1D pipe network flow (Shen et al., 2019). To address these complexities, TUFLOW was selected for this study because of its capability to model surface flow in a 2D domain while also simulating fluvial and pipe networks through its 1D functionality, allowing for dynamic interactions between the two. Moreover, TUFLOW's compatibility with High-performance Computing (HPC) software enables execution on multiple Graphical Processing Units (GPUs), resulting in significantly accelerated model simulation.

To model urban flood dynamics accurately, the configuration included rainfall and tidal boundary conditions, along with a detailed representation of the drainage network. Rainfall data from NOAA Atlas 14 were used to simulate storm events with return periods of 1, 10, 50, and 100 years. Tidal levels, derived from historical storm surge data, were applied as time-varying boundary conditions. These conditions represented the influence of storm tides on both surface and subsurface flooding processes. In the 1D drainage system, dynamic boundary conditions at outfalls reflected time-varying storm tide levels hydrograph. This approach captured the backwater effects and potential reverse flows caused by elevated tides. In the 2D domain, polyline boundary conditions along the coastal edge were used to represent spatially varying tidal forces, ensuring accurate simulation of tidal interactions with the urban landscape. By synchronizing peak storm tide levels with peak rainfall intensities, the model effectively simulated worst-case compound flooding scenarios.

The drainage network was developed using GIS (Geographic Information System) data provided by Norfolk City, comprising 841 pipe sections with a total length of 21.7 km. Pipes smaller than 15 in. in diameter were excluded to focus on the primary stormwater infrastructure. Depth-discharge relationships were applied to pipe connections to simulate the inflow of surface water into the drainage system, while material-specific Manning's roughness coefficients enhanced the accuracy of subsurface flow representation.

The study incorporated storm surge flooding as a critical component of compound flooding scenarios. Historical hurricane data were used to define peak storm tide levels for various return periods, emphasizing the interaction between storm surges and rainfall-driven flooding. These simulations demonstrated the exacerbation of flooding caused by storm surges overwhelming drainage infrastructure and increasing surface water accumulation.

The absence of sea dikes or flood walls along the coastline in the study area allowed for unrestricted tidal interactions, highlighting the increased flood risks in the absence of coastal defenses. The model's design underscored the severe impact of storm surges compared to rainfall-driven flooding alone, emphasizing the need for effective flood management strategies in similar urban coastal environments.

2.5. Designing of combined storm tide and rainfall events

This study analyzes infiltration rates associated with various storm events, focusing on both nuisance flooding in minor events and severe flooding in major and extreme events. Specifically, it examines four storm tide and heavy rainfall events with return periods of 1 year (nuisance flooding), 10 years (major events), and 50 to 100 years (extreme events), based on their probability of exceedance. Additionally, a 2-year return period event was estimated for use in the model evaluation described in Section 3.1, but it is not included in the analysis of infiltration. To evaluate these combined events, we employed the methodology proposed by Shen et al. (2019), which involves analyzing storm tide and heavy rainfall associated with hurricanes in Virginia. Shen et al. (2019) identified historical hurricane data with rainfall and tide peak recurrence intervals exceeding one year in Norfolk. For this study, we selected data from five different hurricanes across five different return periods, including tide level data from the Sewells Point station and rainfall durations ranging from 8 to 77 h, as provided by the National Weather Service (NWS, 2016). Given that the average rainfall duration in the Virginia coastal region is 22 h, a 24-h duration was used for design combined events.

2.5.1. Designing of rainfall events

This study designed heavy rainfall events by considering rainfall intensities across five return periods and the distribution of rainfall over a 24-h period. Precipitation frequency estimates based on Partial-Duration-Series (PDS) data, along with 90 % confidence intervals for this study area, can be accessed on the NOAA Atlas 14 website (link provided in Supplementary Table ST3). The estimated 24-h rainfall intensities with 90 % confidence intervals for the return period of 1, 2, 10, 50 and 100 years are summarized in Table 1.

Based on the rainfall depths and durations from NOAA Atlas 14, Merkel et al. (2015) developed regional rainfall distributions for 17 midwestern and southeastern states, categorizing them into four types. According to these regions, the study area falls within Type C distribution. To generate heavy rainfall events for the respective return periods, the non-dimensional Type C rainfall distribution was multiplied by the 24-h rainfall intensities. Supplementary Figure SF3 illustrates the distributions of these designed 24-h rainfall events.

2.5.2. Designed of storm tide events

Storm tide events were designed by selecting historical peak tide levels from hurricanes that closely matched the return period values within the 95 % confidence intervals, ensuring consistency with rainfall storm events. Historical tide level observations during hurricanes were used to derive annual probability of exceedance curves, with 95 % confidence intervals, for tide levels at Sewells Point, VA. Tide levels were converted from the Mean Higher High Water (MHHW) datum to the North American Vertical Datum of 1988 (NAVD 88). Table 1 summarizes the peak tide levels and their 95 % confidence intervals for the return periods, along with the corresponding hurricanes and their peak tide levels.

2.5.3. Time lag between storm tide and rainfall events

Sixteen compound storm scenarios were developed by Shen et al. (2019), combining heavy rainfall events with storm tide events across various return periods. Their research assessed the impact of time lags between peak rainfall and peak tide levels on flood risk, determining that a lag of −1 to 2 h resulted in the greatest flood volume and inundation area. Considering these findings, this study assumes that peak rainfall coincides with peak tide levels for all scenarios, omitting time lags to represent worst-case flooding conditions.

2.6. Infiltration methodologies for simulating hydrological losses in TUFLOW

TUFLOW offers three methods for modeling water infiltration from the 2D surface into the subsurface: Green-Ampt, Horton, and Initial Loss/Continuing Loss. These methods are designed to simulate hydrological losses, particularly in scenarios where rainfall generates runoff directly on the 2D surface. The infiltration process is tracked in all three methods and stops once the ground becomes saturated. The amount of water that can infiltrate depends on several key factors. These include the loss approach and soil loss parameters, the depth to groundwater or the presence of an impervious layer, the soil's porosity and initial moisture content, and the fraction impervious value of the overlying material layer. The fraction impervious value significantly affects infiltration rates. For example, a completely impervious surface, such as a concrete parking lot, prevents all infiltration, whereas a surface that is 90 % impervious allows for limited infiltration. (TUFLOW manual,

Table 1
24-h rainfall intensity estimates (90 % confidence intervals) and extreme tide levels (95 % confidence intervals) for different return periods, based on NOAA Atlas 14, along with corresponding historical hurricanes.

Return period (probability of exceedance)	1-yr (99 %)	2-yr (50 %)	10-yr (10 %)	50-yr (2 %)	100-yr (1 %)
24-h Rainfall Intensity (mm)	**74**	**91**	**140**	**202**	**234**
90 % Confidence Intervals (mm)	69–81	84–99	129–152	183–218	210–253
Tide Level (m)	**0.78**	**1.1**	**1.56**	**1.87**	**2.06**
95 % Confidence Intervals (m)	0.72–0.81	1.14–1.06	1.35–1.61	1.64–2.33	1.76–2.74
Historical Hurricane Name	Charley (2004)	Unnamed (1937)	Unnamed (1936)	Isabel (2003)	Unnamed (1933)
Historical Peak Tide Level (m)	**0.8**	**1**	**1.56**	**1.91**	**1.95**

2018).

The GA method adjusts the infiltration rate over time based on soil properties such as the soil's hydraulic conductivity, suction, porosity, and initial moisture content. It assumes that as water infiltrates the soil, a boundary forms between the 'dry' soil, which has an initial moisture content, and the 'wet' soil, where the moisture content reaches the soil's porosity (King et al., 1999; TUFLOW manual, 2018). This method offers some advantages over other empirical models. It is a straightforward model, and its parameters can be derived from the soil's physical properties (Gupta, 2017).

The Green-Ampt equation in its fundamental form is represented as follows:

$$\mathrm{f(t)} = \mathrm{K}\left(1 + \frac{\Delta\theta(\varphi + \mathrm{h_0})}{\mathrm{F(t)}}\right) \tag{1}$$

where:

t is time.

K is the saturated hydraulic conductivity.

$\Delta\theta$ is defined as the soil capacity (the difference between the saturated and initial moisture content).

φ is the soil suction head.

h_0 is the depth of ponded water.

$F(t)$ is the cumulative infiltration calculated from:

$$\mathrm{F(t)} - \Delta\theta(\varphi + \mathrm{h_0}) = \mathrm{Kt} \tag{2}$$

The Horton method, in contrast, uses a three-parameter equation to estimate soil infiltration:

$$\mathrm{f(t)} = \mathrm{f_c} + (\mathrm{f_0} - \mathrm{f_c})\,\mathrm{e^{-kt}} \tag{3}$$

where:

f_0 is the initial infiltration rate in mm/h or inches/h.

f_c is the final (indefinite) infiltration rate.

t is time in hours (period of time that the cell is wet).

k is the Horton decay rate.

Unlike the GA method, the parameters f_0 and k cannot be derived from soil water properties and must instead be determined through experimental data (Gupta, 2017). Inaccurate estimation of these parameters can lead to substantial errors in the calculation of infiltration rates, particularly over longer time periods (Raudkivi, 2013).

Finally, The Initial Loss/Continuing Loss (ILCL) method is a simpler approach compared to the GA and Horton infiltration methods. In the ILCL method, water infiltrates based on an initial loss amount, followed by a constant infiltration rate (TUFLOW manual, 2018). While it is less complex, it may not capture the dynamic behavior of infiltration as effectively as the GA and Horton methods.

Given the advantages of the GA method, particularly its direct relationship with soil physical properties, it was chosen to model water infiltration in this study.

3. Results and discussion

3.1. Model evaluation

Evaluating and calibrating urban hydrodynamics models involves comparing their predictions of surface runoff and flooding with observed data, including but not limited to flood depth, extent, and duration particularly in coastal areas (Smith et al., 2011). This process can be challenging due to the often-limited availability of detailed data observations (Helmrich et al., 2021). While calibration is a critical stage in flood modeling, it was not performed in this study due to the lack of detailed flood depth observations necessary to compare with simulated results. Accurate flood depth data typically serves as a foundation for fine-tuning model parameters during calibration. Its absence posed a significant limitation, making a traditional calibration process infeasible. To address this constraint, the model's performance was validated by comparing the predicted inundation maps with flood reports from alternative sources.

These sources included photographs of inundated areas, newspaper articles, interviews, social media, and crowdsourced drone footage, which provide valuable datasets for more comprehensive model evaluations (Fohringer et al., 2015; Loftis et al., 2017; Middleton et al., 2014). Another valuable resource is the mobile navigation app Waze, owned by Google. In addition to reporting road closures and traffic congestion, Waze also collects real-time reports on flood incidents. Through its Waze for Cities data-sharing program, the app provides aggregated user-reported data on flooding, which is accessible to public entities worldwide (Praharaj et al., 2021). These sources provided valuable spatial and temporal flood data through community and driver reports, demonstrating the utility of crowdsourced and observational datasets for model evaluation.

To assess the model's performance, we compared maximum inundation maps with flood report data from both Waze and Norfolk's System to Track, Organize, Record, and Map (STORM) application. The STORM dataset, updated since 2010, includes reports on weather-related incidents such as flooded streets, damaged trees, disabled vehicles, and downed cables, collected by residents and city staff during and after inclement weather (available at https://data.norfolk.gov/Maps/STORM-MAP/fefd-kf5s). For all simulations, we focused on ponding depths exceeding 10 cm. This threshold was selected based on the assumption that flood impacts become significant at this depth, distinguishing between minor surface water accumulation and more substantial inundation that could potentially affect land use and infrastructure (Shen et al., 2019). We analyzed timestamped, location-specific flood reports from four selected neighborhoods. Community reports were gathered over a ten-year period (2010–2019), while driver reports were collected over two years (2018–2019). To account for the differing time spans of these datasets and to create a more conservative scenario, we selected a storm event with a 2-year return period for analysis, as described in section 2.3 (Supplementary Figure SF3 and Table 1). A flood report, whether from a community member or a driver, was considered to validate the model simulation if the simulated ponding depth occurred within a 20-m buffer of the reported flood location. This buffer distance, adopted from Shen et al. (2019), was chosen because it effectively captures areas immediately adjacent to the analyzed features while minimizing overlap, thus ensuring a balance between spatial coverage and precision. The choice of buffer zone introduces uncertainty, as varying the buffer distance affects the sample size of reports. Larger buffers tend to increase the sample size but may reduce spatial accuracy by including unrelated features. On the other hand, smaller buffers improve spatial precision but may exclude relevant data points, leading to a reduced sample size. Given these considerations, the 20-m buffer was retained as it provides an optimal trade-off between spatial accuracy and sample size.

We obtained 60 flood reports from the community and 74 from drivers, all categorized under the "street flooded" attribute. To avoid duplication, we eliminated overlapping points, assuming the reports referred to the same locations. Supplementary Table ST4 presents the spatiotemporal distribution of the reports. Among the community reports, 53 out of 60 (88 %) matched the locations predicted by the flood model simulation. Similarly, 66 out of 74 driver reports (89 %) matched the predicted locations. These high match percentages indicate a strong correlation between observed flood events and our model's predictions, underscoring the model's accuracy and reliability in identifying flood-prone areas.

Most matched points were in the southern part of the study domain, specifically in the Park Place and Kensington neighborhoods, which are the most impervious regions and are near the Lafayette River, an area vulnerable to sea level rise. The remaining unmatched points were, on average, 40 m away from the reported locations, as illustrated by two examples from the community reports (Fig. 2A) and driver reports (Fig. 2B). Additionally, colleagues from other institutions, who are familiar with the area and involved in a related project, provided valuable feedback. Their input validated the model and offered further useful insights.

While the crowdsourced flood report dataset provides valuable street-level information, it has notable limitations. Reports collected from community members and drivers using the Waze application include only the date and location of flooding, lacking detailed information on flood depth or timing. Additionally, as with most crowdsourced data, these reports are subject to inherent subjectivity and bias, as they are submitted by individual users (Sadler et al., 2018). However, given the most reliable information available for model evaluation, it is reasonable to conclude that the urban flood model effectively predicts flooded roads during various storm events (Shen et al., 2019).

3.2. Flood extension and volume in saturated conditions

This section examines how flooding extends and volume change under fully saturated conditions. We analyze maximum ponding depths across the four combined storm events corresponding to the 1-, 10-, 50-, and 100-year return periods. Fig. 3 presents the spatial distribution of ponding depths at peak inundation under varying saturation levels. At 100 % saturation, the maximum depths of 4.0, 5.0, 5.42, and 5.47 m were recorded during compound storms associated with the 1-, 10-, 50-, and 100-year return periods tide and rainfall events, respectively. These depths occur at three critical underpasses located in the Park Place and Kensington areas, which significantly contribute to the overall ponding. While pumps are used in practice to drain these underpasses, they were not included in the model, leading to potentially higher simulated flood depths. When excluding the underpasses, the maximum ponding depths were 2.0, 2.7, 3.1, and 3.15 m for the same storm events.

Near the shoreline, the ponding depth increases rapidly, reaching depths >1 m. In the rest of the domain, inundation is more concentrated in the Park Place and Kensington neighborhoods and less concentrated in the Colonial Place and Riverwood neighborhoods.

The storm scenario with a 1-year return period for rainfall and storm tide associated with a nuisance flooding event would flood 10.4 % of the land area with an estimated flow volume of about 0.195 million cubic meters. For the major and more extreme scenarios, the model predicts the following impacts:

1) A 10-year return period (major event) storm would flood approximately 19 % of the land area, with a flow volume of about 0.47 million cubic meters.
2) A 50-year return period (extreme event) storm would flood around 28 % of the land area, with a flow volume of approximately 0.76 million cubic meters.

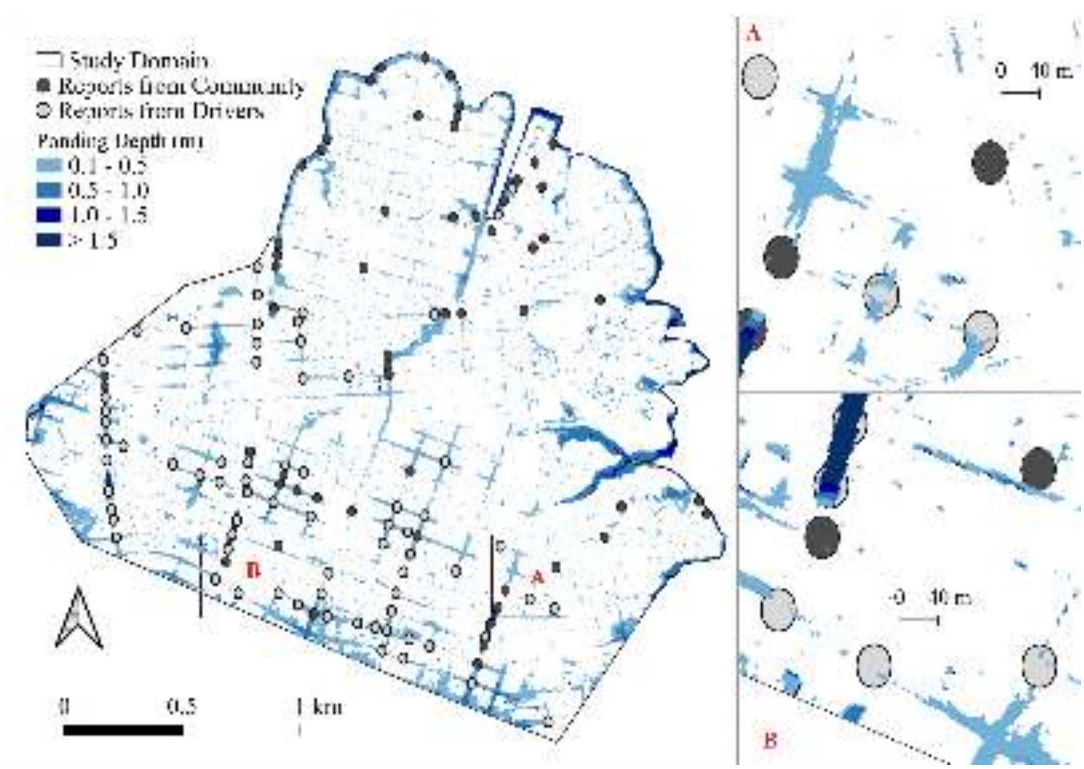

Fig. 2. Maximum inundation map showing ponding depths and flood report locations from community and driver reports in Norfolk for a 2-year return period event. (a) Community report locations and model predictions, with unmatched points averaging 40 m away. (b) Driver report locations and model predictions, also showing a similar 40-m discrepancy for unmatched points.

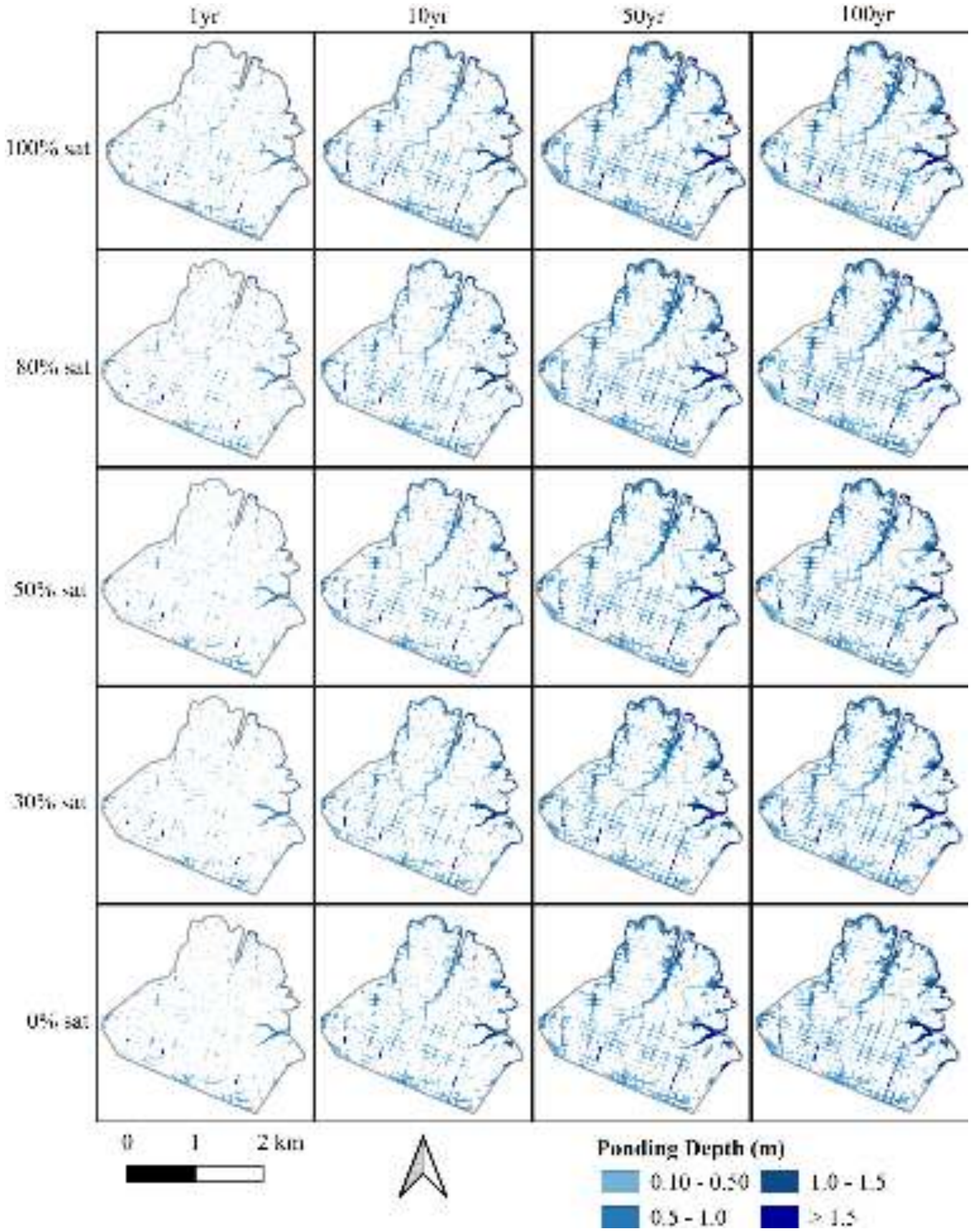

Fig. 3. Effect of storm tide and heavy rainfall on flood ponding depth at peak inundation, assuming different initial soil saturated conditions (100 %, 80 %, 50 %, 30 %, 0 %) across various return periods.

3) A 100-year return period (extreme event) storm, which represents the most severe scenario, would flood about 29.6 % of the land area, with a flow volume of approximately 0.79 million cubic meters.

3.3. Flood extension and volumes considering different saturation conditions

To assess the role of infiltration in flood dynamics, we conducted simulations under four different saturations levels: 80 %, 50 %, 30 %, and 0 % (Fig. 3). These conditions were adjusted by modifying soil porosity to accurately reflect the soil's water absorption capacity. We estimated that, under high hydraulic conductivity conditions, water could infiltrate to a depth of 27 cm within 25 h. Therefore, this thickness was selected for use in our study to assess how different levels of soil saturation influence flood extent and runoff.

The most significant changes in flooded areas occur during the 1-year return period, where reductions in soil saturation result in notable increases in flood extent. In contrast, for the 10-, 50-, and 100-year return periods, the differences in flooded area are minimal, suggesting that soil saturation levels have a more pronounced impact during less extreme storm events. This is evident in Fig. 3, where the effects of varying saturation are clearly observable for the 1-year return period, while the changes are less distinct for the major and extreme scenarios.

To quantify these changes, Table 2 presents the reduction in flooded areas (in km^2) and flooded volumes (in million cubic meters) under different saturation conditions across various return periods. The table also highlights the total reductions in both flooded area and volume, accounting for infiltration losses when comparing saturated and unsaturated conditions.

For the 1-year return period, infiltration significantly reduces the

Table 2
Reduction in flooded area and volume across different saturation conditions and return periods.

Return period	Flooded area (km^2)					Total decrease	Flooded volume (million cubic meters)					Total decrease
	100 %	80 %	50 %	30 %	0 %		100 %	80 %	50 %	30 %	0 %	
1 yr	0.53	0.49	0.41	0.38	0.35	33 %	0.195	0.182	0.156	0.148	0.138	29 %
10 yr	1	0.98	0.93	0.9	0.88	12 %	0.472	0.464	0.442	0.431	0.421	11 %
50 yr	1.42	1.37	1.34	1.31	1.29	9 %	0.762	0.726	0.712	0.700	0.690	9 %
100 yr	1.5	1.49	1.47	1.44	1.42	5 %	0.799	0.793	0.782	0.770	0.760	5 %

flooded area by 33 %. This substantial reduction highlights the crucial role of infiltration in managing nuisance flooding, where soil absorption can effectively mitigate flood extent in less severe storms. The significant impact of infiltration for the 1-year event is attributed to the relatively lower volume of water and slower runoff, allowing the soil to absorb a more considerable portion of the precipitation. In comparison, for the 10-, 50-, and 100-year events, the reductions are smaller, at 12 %, 9 %, and 5 %, respectively.

Supplementary Figure SF4 further illustrates how the inundation area varies with saturation levels and water depths during the nuisance flooding event. At 100 % and 80 % saturation, inundation is extensive, particularly in areas with shallow ponding depths (0.10–0.30 m) and moderate depths (0.30–0.50 m), as indicated by the prevalence of yellow and red zones. Deeper water depths (0.50–0.60 m and > 0.60 m) appear primarily in localized low-lying areas, such as underpasses and zones with high development intensity, where infiltration is less effective.

As saturation decreases, the inundation area is visibly reduced, especially in shallow water zones. At 50 % saturation, infiltration significantly reduces flood extent in regions with ponding depths of 0.10–0.30 m. By 30 % saturation, this reduction becomes even more pronounced, with many formerly inundated shallow areas no longer visible on the map.

At 0 % saturation, the inundation area is minimal, with water depths largely confined to localized depressions or poorly drained regions. Most shallow water zones (0.10–0.30 m) are almost entirely mitigated, while only small pockets of moderate (0.30–0.50 m) and deep ponding (>0.50 m) remain.

The Supplementary Figure SF4 highlights that flood mitigation through infiltration is most effective in reducing shallow inundation areas, particularly under lower saturation conditions. Conversely, areas with greater water depths tend to persist, as water concentrates in low-lying or highly impervious zones where infiltration is limited.

Infiltration's impact on inundation volume is equally significant and complements the analysis of flooded areas. As presented in Table 2, the 1-year return period event shows a marked reduction in flood volume, decreasing from 0.195 million cubic meters (100 % saturation) to 0.138 million cubic meters (0 % saturation), representing a 29 % reduction. This substantial decrease highlights the effectiveness of infiltration in mitigating flood risks during nuisance events. The pronounced effect of infiltration during the 1-year event can be attributed to the relatively low water volumes associated with such events, allowing sufficient time for soil absorption before saturation limits are reached. Additionally, the slower runoff velocities characteristic of nuisance flooding contributes to greater infiltration opportunities, further reducing the inundation volume.

In contrast, for higher return periods (10-, 50-, and 100-year events), the reductions in inundation volume are less significant, with decreases of 11 %, 9 %, and 5 %, respectively. The diminishing influence of infiltration on flood volume for extreme events stems from the overwhelming water inputs that quickly saturate the soil, leaving minimal capacity for additional absorption. Consequently, runoff becomes the dominant factor driving flood volumes in these scenarios.

3.4. Analysis of infiltration dynamics across different storm intensities

Supplementary Figure SF5 illustrates the spatial distribution of infiltration losses after 12.5 h of simulation time within the study domain for the selected return periods. This time point is chosen because it captures the peak intensity of the storm events, which is the most critical time point for assessing infiltration and runoff dynamics. The spatial variability of these losses is strongly correlated with the distribution of impervious surfaces, land cover types, and material properties across the area. Areas with high imperviousness, such as roads and built-up environments, exhibit minimal infiltration, leading to increased surface runoff. Conversely, regions with more pervious surfaces, such as parks and open spaces, show higher infiltration rates, which contribute to reduced surface water accumulation.

For a more detailed analysis, a specific profile within the study domain was examined to assess infiltration rates under controlled conditions. This profile, located in Lafayette Park, was selected due to its homogeneous material type and high perviousness, offering a clearer understanding of infiltration dynamics without the confounding effects of varying soil properties. Fig. 4a presents a cross-section characterized by uniform soil and material conditions, allowing for an in-depth analysis of infiltration rates over time.

The analysis reveals that infiltration rates decrease as storm intensity increases, a trend clearly illustrated in Fig. 5. Average infiltration rates are 17.2 mm/h for nuisance flooding events and 14.7 mm/h, 13.5 mm/h, and 13 mm/h for the major and two extreme events respectively. During larger storm events, the soil and stormwater infrastructure reach saturation more quickly, reducing the capacity for additional water absorption and leading to increased runoff. The decrease in infiltration rates during larger storms is indicative of the soil's limited capacity to absorb water once it approaches saturation, causing excess runoff to contribute more significantly to flooding. This observation aligns with the findings of Hossain Anni et al. (2020), which emphasized the significant impact of storm intensity on infiltration dynamics. Similarly, Ryan et al. (2022) highlighted that model results across a mixed catchment basins are particularly sensitive to infiltration rates, especially under conditions of relatively low rainfall intensity. The reduced infiltration during extreme events underscores the importance of considering soil saturation levels when assessing flood risks, particularly in highly impervious urban areas.

Furthermore, the cumulative infiltration data in Fig. 5 provides insights into the total volume of water absorbed by the soil throughout the storm events. The data show that during nuisance flooding events, the soil reaches saturation more gradually, allowing for effective water absorption over time without fully saturating. Similarly, for the 10-year return period event, fully saturated conditions are not reached within 25 h, indicating that the soil retains some capacity to absorb water over a more extended period during less intense storms.

In contrast, for the more intense 50- and 100-year return period events, the soil reaches saturation much more quickly—approximately 17 h for the 50-year event and 16 h for the 100-year event. This rapid saturation during extreme storms highlights the limited capacity of both the soil and stormwater infrastructure to absorb additional water, resulting in increased surface runoff and a higher risk of flooding.

This analysis underscores the importance of incorporating detailed infiltration data into urban flood models, particularly in coastal cities

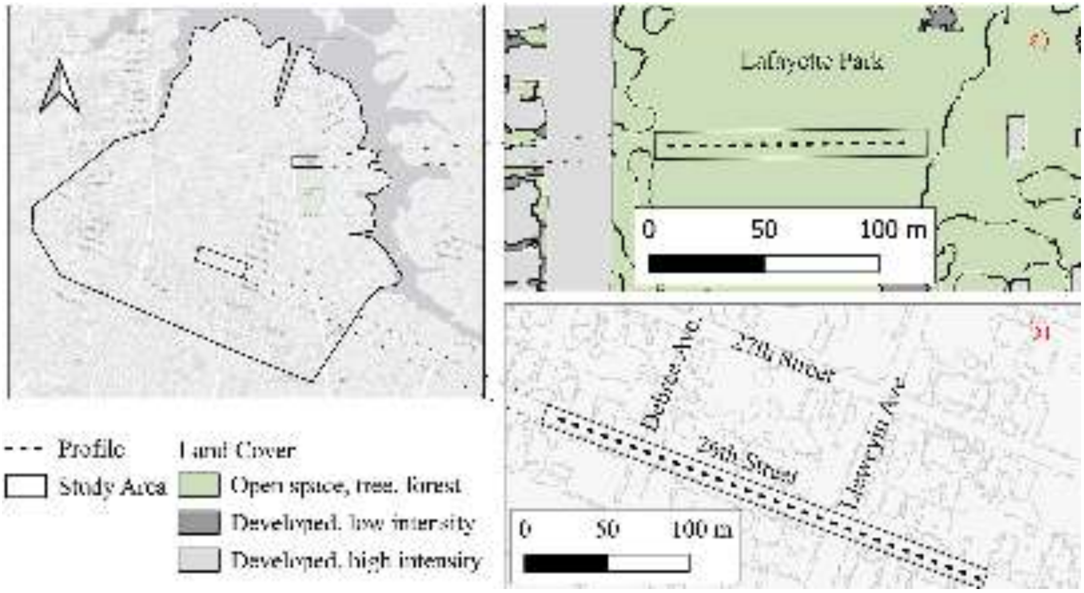

Fig. 4. a) Cross-section of a uniform infiltration profile in Lafayette Park, illustrating infiltration dynamics. (b) Cross-section of West 26th Street, showing the flood profile during a 1-year return period event, assessing the impact of infiltration on overland flow.

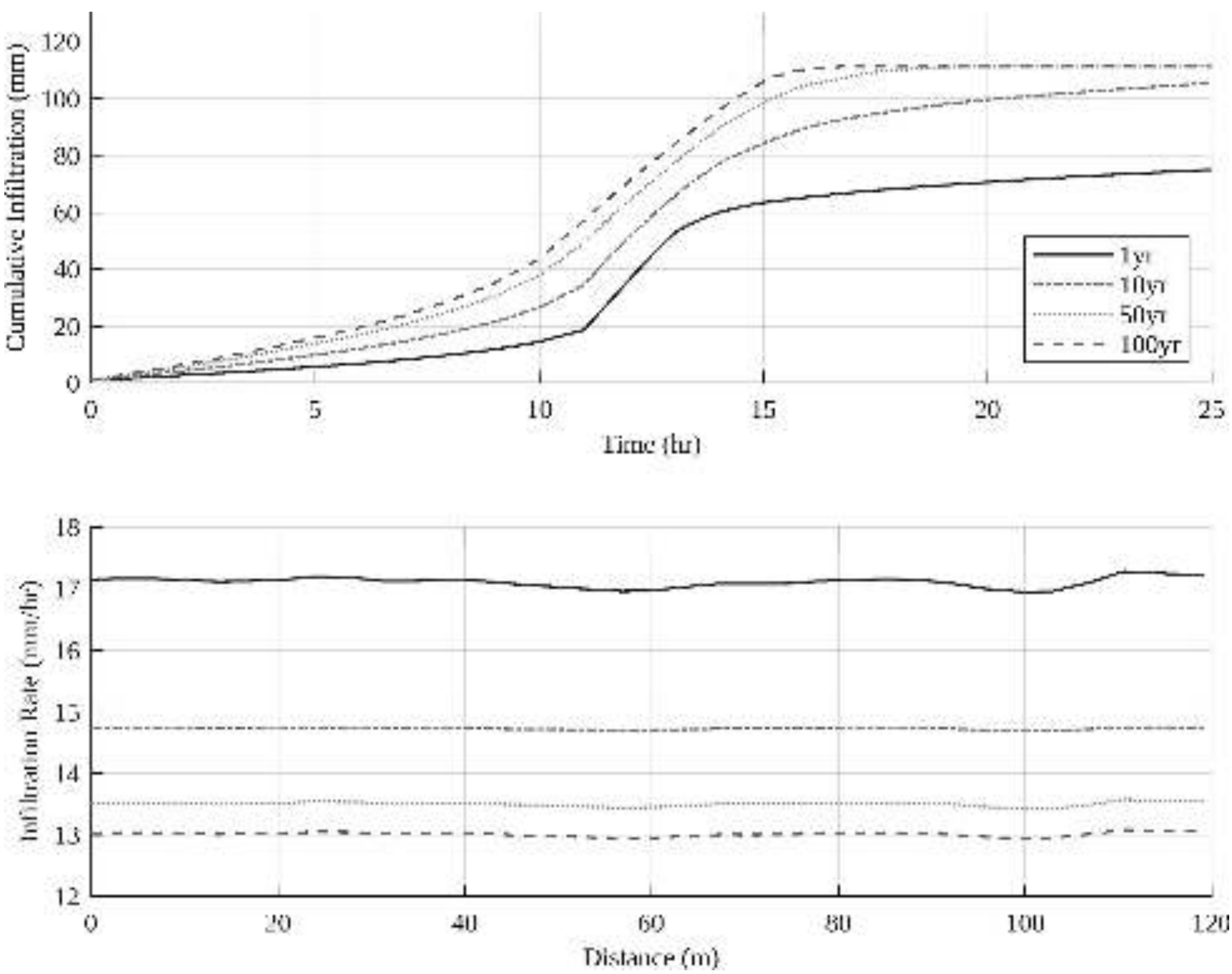

Fig. 5. Infiltration rates and cumulative infiltration across different return periods, highlighting variations across minor, major, and extreme scenarios at the cross-section in Lafayette Park.

where nuisance flooding events occur. In such scenarios, infiltration plays a significant role, and the combination of storm tide and heavy rainfall can lead to complex flood dynamics.

3.5. Overland flood profile differences under various saturation conditions

To assess the impact of varying saturation conditions on the overland flood profile for the 1-year return period event, we selected a street in the Park Place neighborhood, an area characterized by high imperviousness. The 1-year return period was chosen because infiltration has a more pronounced effect during such events compared to the more extreme 10-, 50-, and 100-year return periods. Infiltration's influence is notably significant in less intense storms, where it can meaningfully reduce surface runoff. Specifically, our analysis focuses on West 26th Street between Debree and Lleweyin Avenues, as illustrated in Fig. 4b.

Fig. 6 shows the five different profiles under varying saturation conditions. The graph illustrates how water depth above the DEM changes with distance for saturation levels of 100 %, 80 %, 50 %, 30 %, and 0 %. The largest difference in water depth between the 100 % and 0 % saturation conditions reaches just under 0.2 m around the 150-m mark. This indicates that infiltration has a significant impact on water depth, especially in highly impervious areas like West 26th Street in the Park Place neighborhood. The variability in water depth across different saturation levels further underscores the importance of accounting for infiltration effects when assessing flood risks and developing mitigation strategies.

3.6. Study limitations and opportunities for future research

This study acknowledges some limitations, including the lack of detailed temporal flood depth data from community reports, which could further enhance model calibration and validation. Additionally, the hydrodynamic model's simplifications, such as the exclusion of small-scale drainage structures, pumps, and the influence of groundwater dynamics, may have affected the accuracy of flood extent and volume predictions in localized areas. Future work should explore the integration of real-time monitoring systems, such as street-level sensors and remote sensing technologies, to capture dynamic flood behavior more accurately. Expanding the analysis to include additional storm scenarios, particularly those observing the effects of climate change on rainfall intensity, sea-level rise, and storm surge interactions, would provide deeper insights into evolving flood risks. Incorporating groundwater processes into hydrodynamic models would further improve their accuracy by accounting for interactions between infiltration, subsurface flow, and surface runoff. Furthermore, incorporating socio-economic data could facilitate a more comprehensive assessment of flooding impacts and inform the development of equitable and effective mitigation strategies.

4. Conclusions

In this study, we developed a 2D/1D hydrodynamic model to evaluate the role of infiltration across different flood events. The results emphasize the significant impact of infiltration on nuisance flooding events, while its effect on major and extreme events is minimal in comparison. Key findings are summarized as follows:

(1) During a nuisance flooding event (1-year return period), infiltration losses significantly reduce the extent of urban flooding by 33 % when comparing saturated to unsaturated conditions. This finding emphasizes the importance of incorporating infiltration processes in flood risk assessments for short-term events.
(2) For events with longer return periods (10-, 50-, and 100-years return periods), associated with major and extreme flooding events, the impact of infiltration losses on flood extent is minimal compared with a nuisance flooding event, with reductions of 12 %, 9 % and 5 % respectively. This suggests that during extreme events, factors such as surface runoff and overflow become more dominant in influencing flooding. In terms of flooded volume, the 1-year return period event showed a significant reduction due to infiltration, decreasing from 0.195 million cubic meters (100 % saturation) to 0.138 million cubic meters (0 % saturation), a 29 % reduction. This highlights infiltration's critical role in managing nuisance flooding by enabling sufficient soil absorption and reducing runoff. For longer return periods (10-, 50-, and 100-year

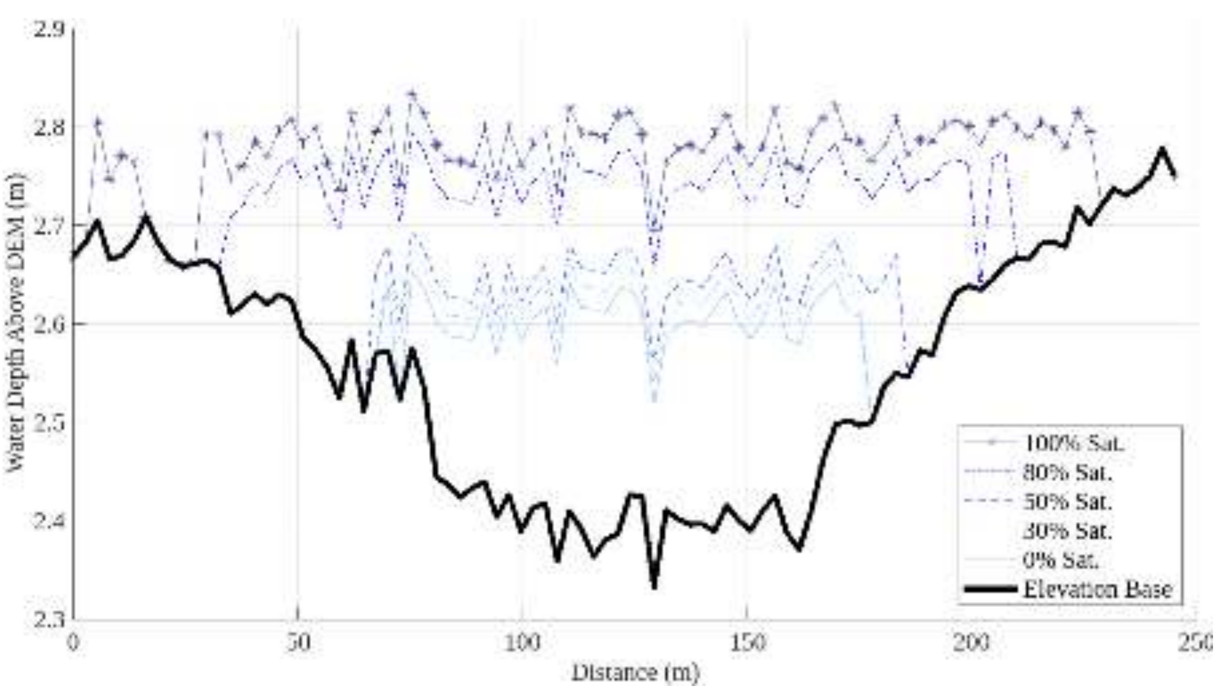

Fig. 6. Profiles illustrating the variations in inundation under different saturation conditions for the 1-year return period associated with nuisance flooding at the West 26th Street cross-section.

events), volume reductions were smaller—11 %, 9 %, and 5 %, respectively—owing to the rapid saturation of the soil by overwhelming water inputs.

(3) Analysis of flood profiles along a street in the Park Place neighborhood demonstrates significant variability in water depth under different saturation conditions. The most notable difference, approaching 20 cm, occurs between 100 % and 0 % saturation for the 1-year return period. This highlights the critical importance of accounting for infiltration effects, especially in highly impervious areas, when conducting flood risk assessments and developing effective mitigation strategies.

(4) It was observed that during 1-year and 10-year return period events, full soil saturation is not reached within the observed time frame. This indicates that the infiltration capacity of urban soils can manage moderate rainfall events without becoming saturated, thereby mitigating flood risks.

(5) Variations in soil permeability and land use significantly impact infiltration rates and resulting flood extents. This emphasizes the need for detailed local data to accurately assess and manage flood risks.

(6) The study highlights the importance of incorporating community-provided data in evaluating 1D/2D hydrodynamic models. Local reports offer valuable insights that can complement traditional sources, enhancing flood modeling and management effort.

Overall, the findings of this study provide valuable insights for improving flood resilience in urban coastal areas and developing more effective disaster mitigation strategies.

CRediT authorship contribution statement

Sergio A. Barbosa: Writing – review & editing, Writing – original draft, Visualization, Validation, Software, Methodology, Investigation, Formal analysis, Data curation, Conceptualization. **Yidi Wang:** Writing – review & editing, Writing – original draft, Methodology, Investigation. **Jonathan L. Goodall:** Supervision, Resources, Methodology, Investigation, Funding acquisition, Formal analysis, Conceptualization.

Declaration of Generative AI and AI-assisted technologies in the writing process

During the preparation of this work, the authors used Chat-GPT to improve readability. After using this tool/service, the authors reviewed and edited the content as needed and take full responsibility for the content of the publication.

Funding sources

This study was supported by the National Science Foundation under Grant No. 2209139 “Enhancing Resilience and Equity in Urban Coastal Communities through the Co-Generation of Community Capitals”.

Declaration of competing interest

The authors declare that they have no known competing financial interests or personal relationships that could have appeared to influence the work reported in this paper.

Appendix A. Supplementary data

Supplementary data to this article can be found online at https://doi.org/10.1016/j.scitotenv.2025.178908.

Data availability

Data will be made available on request.

References

Agbola, B.S., Ajayi, O., Taiwo, O.J., Wahab, B.W., 2012. The august 2011 flood in Ibadan, Nigeria: anthropogenic causes and consequences. Int. J. Disaster Risk Sci. 3 (4), 207–217. https://doi.org/10.1007/s13753-012-0021-3.

Archetti, R., Bolognesi, A., Casadio, A., Maglionico, M., 2011. Development of flood probability charts for urban drainage network in coastal areas through a simplified joint assessment approach. Hydrol. Earth Syst. Sci. 15 (10), 3115–3122. https://doi.org/10.5194/hess-15-3115-2011.

Bacopoulos, P., Tang, Y., Wang, D., Hagen, S.C., 2017. Integrated hydrologic-hydrodynamic modeling of estuarine-riverine flooding: 2008 tropical storm fay. J. Hydrol. Eng. 22 (8). https://doi.org/10.1061/(ASCE)HE.1943-5584.0001539.

Brown, L., Murray, V., 2013. Examining the relationship between infectious diseases and flooding in Europe: a systematic literature review and summary of possible public health interventions. Disaster Health 1 (2), 117–127. https://doi.org/10.4161/dish.25216.

C2ES, 2023. Drought and Climate Change. https://www.c2es.org/content/drought-and-climate-change/ (accessed 26 December 2024).

Curriero, F.C., Patz, J.A., Rose, J.B., Lele, S., 2001. The association between extreme precipitation and waterborne disease outbreaks in the United States, 1948-1994. Am. J. Public Health 91 (8), 1194–1199. https://doi.org/10.2105/ajph.91.8.1194.

Dawson, R.J., Speight, L., Hall, J.W., Djordjevic, S., Savic, D., Leandro, J., 2008. Attribution of flood risk in urban areas. J. Hydroinf. 10 (4), 275–288. https://doi.org/10.2166/hydro.2008.054.

E P A, 2018. Storm Water Management Model (SWMM) | US EPA. https://www.epa.gov/water-research/storm-water-management-model-swmm (accessed 26 April 2024).

Fan, Y., Ao, T., Yu, H., Huang, G., Li, X., 2017. A coupled 1D-2D hydrodynamic model for urban flood inundation. Adv. Meteorol. 2017, 1–12. https://doi.org/10.1155/2017/2819308.

Fernández, D.S., Lutz, M.A., 2010. Urban flood hazard zoning in Tucumán Province, Argentina, using GIS and multicriteria decision analysis. Eng. Geol. 111 (1–4), 90–98. https://doi.org/10.1016/j.enggeo.2009.12.006.

Fohringer, J., Dransch, D., Kreibich, H., Schröter, K., 2015. Social media as an information source for rapid flood inundation mapping. Nat. Hazards Earth Syst. Sci. 15 (12), 2725–2738. https://doi.org/10.5194/nhess-15-2725-2015.

Gupta, R.S., 2017. Hydrology and hydraulic systems. books.google.com.

Helmrich, A.M., Ruddell, B.L., Bessem, K., Chester, M.V., Chohan, N., Doerry, E., Eppinger, J., Garcia, M., Goodall, J.L., Lowry, C., Zahura, F.T., 2021. Opportunities for crowdsourcing in urban flood monitoring. Environ. Model Softw. 143, 105124. https://doi.org/10.1016/j.envsoft.2021.105124.

Hoang, L., Fenner, R.A., 2016. System interactions of stormwater management using sustainable urban drainage systems and green infrastructure. Urban Water J. 13 (7), 739–758. https://doi.org/10.1080/1573062X.2015.1036083.

Hossain Anni, A., Cohen, S., Praskievicz, S., 2020. Sensitivity of urban flood simulations to stormwater infrastructure and soil infiltration. J. Hydrol. 588, 125028. https://doi.org/10.1016/j.jhydrol.2020.125028.

Huong, H.T.L., Pathirana, A., 2013. Urbanization and climate change impacts on future urban flooding in Can Tho city, Vietnam. Hydrol. Earth Syst. Sci. 17 (1), 379–394. https://doi.org/10.5194/hess-17-379-2013.

Karamouz, M., Razmi, A., Nazif, S., Zahmatkesh, Z., 2017. Integration of inland and coastal storms for flood hazard assessment using a distributed hydrologic model. Environ. Earth Sci. 76 (11), 395. https://doi.org/10.1007/s12665-017-6722-6.

King, K.W., Arnold, J.G., Bingner, R.L., Infiltration, Modeling, 1999. Comparison of Green-Ampt and curve number methods on Goodwin Creek watershed using SWAT. Trans. ASABE 42 (4), 919–925.

Leandro, J., Chen, A.S., Djordjević, S., Savić, D.A., 2009. Comparison of 1D/1D and 1D/2D coupled (sewer/surface) hydraulic models for urban flood simulation. J. Hydraul. Eng. 135 (6), 495–504. https://doi.org/10.1061/(ASCE)HY.1943-7900.0000037.

Li, H., Lin, L., Burks-Copes, K.A., 2013. Modeling of coastal inundation, storm surge, and Relative Sea-level rise at Naval Station Norfolk, Norfolk, Virginia, U.S.a. J. Coast. Res. 286, 18–30. https://doi.org/10.2112/JCOASTRES-D-12-00056.1.

Loftis, J.D., Wang, H., Forrest, D., Rhee, S., Nguyen, C., 2017. Emerging flood model validation frameworks for street-level inundation modeling with StormSense. In: Proceedings of the 2nd international workshop on science of Smart City operations and platforms engineering - SCOPE, 17, pp. 13–18. https://doi.org/10.1145/3063386.3063764.

Mahmood, M.I., Elagib, N.A., Horn, F., Saad, S.A.G., 2017. Lessons learned from Khartoum flash flood impacts: an integrated assessment. Sci. Total Environ. 601–602, 1031–1045. https://doi.org/10.1016/j.scitotenv.2017.05.260.

Mahmoud, S.H., Gan, T.Y., 2018. Urbanization and climate change implications in flood risk management: developing an efficient decision support system for flood susceptibility mapping. Sci. Total Environ. 636, 152–167. https://doi.org/10.1016/j.scitotenv.2018.04.282.

Martins, R., Leandro, J., Djordjevic, S., 2016. Influence of sewer network models on urban flood damage assessment based on coupled 1D/2D models. J. Flood Risk Manag. 11. https://doi.org/10.1111/jfr3.12244.

McCuen, R.H., 1998. Hydrologic Analysis and Design, Second. ed. Prentice Hall, New Jersey.

Merkel, W., Helen, M., Quan, Q., 2015. Design Rainfall Distributions Based on NOAA Atlas 14 Rainfall Depths and Durations. Beltsville, MD.

Middleton, S.E., Middleton, L., Modafferi, S., 2014. Real-time crisis mapping of natural disasters using social media. IEEE Intell. Syst. 29 (2), 9–17. https://doi.org/10.1109/MIS.2013.126.
Mignot, E., Dewals, B., 2022. Hydraulic modelling of inland urban flooding: recent advances. J. Hydrol. 609, 127763. https://doi.org/10.1016/j.jhydrol.2022.127763.
Moftakhari, H.R., AghaKouchak, A., Sanders, B.F., Allaire, M., Matthew, R.A., 2018. What is nuisance flooding? defining and monitoring an emerging challenge. Water Resour. Res. 54 (7), 4218–4227. https://doi.org/10.1029/2018WR022828.
National Weather Service. Definitions and general terminology, Hydrologic services program NWSPD 10–9, Natl. WeatherServ. https://www.weather.gov/directives/. 2012 (accessed 31 March 2024).
Ntelekos, A.A., Oppenheimer, M., Smith, J.A., Miller, A.J., 2010. Urbanization, climate change and flood policy in the United States. Clim. Chang. 103 (3–4), 597–616. https://doi.org/10.1007/s10584-009-9789-6.
NWS, 2016. The hurricane history of central and eastern Virginia. https://www.weather.gov/media/akq/miscNEWS/hurricanehistory.pdf.
Praharaj, S., Chen, T.D., Zahura, F.T., Behl, M., Goodall, J.L., 2021. Estimating Impacts of Recurring Flooding on Roadway Networks: A Norfolk, Virginia case study. Natural Hazards. https://doi.org/10.1007/s11069-020-04427-5.
Raudkivi, A.J., 2013. Hydrology: an advanced introduction to hydrological processes and modelling. books.google.com.
Ray, T., Stepinski, E., Sebastian, A., Bedient, P.B., 2011. Dynamic modeling of storm surge and inland flooding in a Texas coastal floodplain. J. Hydraul. Eng. 137 (10), 1103–1110. https://doi.org/10.1061/(ASCE)HY.1943-7900.0000398.
Russo, B., Sunyer, D., Velasco, M., Djordjević, S., 2015. Analysis of extreme flooding events through a calibrated 1D/2D coupled model: the case of Barcelona (Spain). J. Hydroinf. 17 (3), 473–491. https://doi.org/10.2166/hydro.2014.063.
Ryan, P., Syme, B., Gao, S., Collecutt, G., 2022. Direct Rainfall Hydraulic Model Validation. In: Proceedings of the 2014 Hydrology and Water Resources Symposium. Engineers Australia, Perth, Australia.
Sadler, J.M., Goodall, J.L., Morsy, M.M., Spencer, K., 2018. Modeling urban coastal flood severity from crowd-sourced flood reports using Poisson regression and random Forest. J. Hydrol. 559, 43–55. https://doi.org/10.1016/j.jhydrol.2018.01.044.
Sadler, Jeffrey M., Haselden, N., Mellon, K., Hackel, A., Son, V., Mayfield, J., Blase, A., Goodall, J.L., 2017. Impact of sea-level rise on roadway flooding in the Hampton roads region, Virginia. J. Infrastruct. Syst. 23 (4). https://doi.org/10.1061/(ASCE)IS.1943-555X.0000397.
Seyoum, S.D., Vojinovic, Z., Price, R.K., Weesakul, S., 2012. Coupled 1D and noninertia 2D flood inundation model for simulation of urban flooding. J. Hydraul. Eng. 138 (1), 23–34. https://doi.org/10.1061/(ASCE)HY.1943-7900.0000485.
Shen, Y., Morsy, M.M., Huxley, C., Tahvildari, N., Goodall, J.L., 2019. Flood risk assessment and increased resilience for coastal urban watersheds under the combined impact of storm tide and heavy rainfall. J. Hydrol. 579, 124159. https://doi.org/10.1016/j.jhydrol.2019.124159.
Shen, Y., Tahvildari, N., Morsy, M.M., Huxley, C., Chen, T.D., Goodall, J.L., 2022. Dynamic modeling of inland flooding and storm surge on coastal cities under climate change scenarios: transportation infrastructure impacts in Norfolk, Virginia USA as a case study. Geosciences 12 (6), 224. https://doi.org/10.3390/geosciences12060224.
Silva-Araya, W., Santiago-Collazo, F., Gonzalez-Lopez, J., Maldonado-Maldonado, J., 2018. Dynamic modeling of surface runoff and storm surge during hurricane and tropical storm events. Hydrology 5 (1), 13. https://doi.org/10.3390/hydrology5010013.
Smith, R.A.E., Bates, P.D., Hayes, C., 2011. Evaluation of a coastal flood inundation model using hard and soft data. Environ. Model Softw. https://doi.org/10.1016/j.envsoft.2011.11.008.
Syme, W.J., 2001. TUFLOW–two & one-dimensional unsteady FLOW software for Rivers, estuaries and coastal waters. Paper presented at the IEAust water panel seminar and workshop on 2d flood modelling, Australia, Sydney, 2001, pp. 2–9.
Tabari, H., 2020. Climate change impact on flood and extreme precipitation increases with water availability. Sci. Rep. 10 (1), 13768. https://doi.org/10.1038/s41598-020-70816-2.
Tahvildari, N., Abi Aad, M., Sahu, A., Shen, Y., Morsy, M., Murray-Tuite, P., Goodall, J.L., Heaslip, K., Cetin, M., 2022. Quantification of compound flooding over roadway network during extreme events for planning emergency operations. Nat. Hazards Rev. 23 (2). https://doi.org/10.1061/(ASCE)NH.1527-6996.0000524.
Tan, Y., Cheng, Q., Lyu, F., Liu, F., Liu, L., Su, Y., Yuan, S., Xiao, W., Liu, Z., Chen, Y., 2024. Hydrological reduction and control effect evaluation of sponge city construction based on one-way coupling model of SWMM-FVCOM: a case in university campus. J. Environ. Manag. 349, 119599. https://doi.org/10.1016/j.jenvman.2023.119599.
Teng, J., Jakeman, A.J., Vaze, J., Croke, B.F.W., Dutta, D., Kim, S., 2017. Flood inundation modelling: a review of methods, recent advances and uncertainty analysis. Environ. Model Softw. 90, 201–216. https://doi.org/10.1016/j.envsoft.2017.01.006.
Tran, T.-N.-D., Tapas, M.R., Do, S.K., Etheridge, R., Lakshmi, V., 2024. Investigating the impacts of climate change on hydroclimatic extremes in the tar-Pamlico River basin, North Carolina. J. Environ. Manag. 363, 121375. https://doi.org/10.1016/j.jenvman.2024.121375.
TUFLOW manual, 2018. TUFLOW Classic/HPC User Manual.
Tunstall, S., Tapsell, S., Green, C., Floyd, P., George, C., 2006. The health effects of flooding: social research results from England and Wales. J. Water Health 4 (3), 365–380. https://doi.org/10.2166/wh.2006.031.
Tyndall Centre, 2021. Climate change increases extreme rainfall and thechance of floods. https://tyndall.ac.uk/ (accessed 26 December 2024).
Upadhyaya, J.K., Biswas, N., Tam, E., 2014. A review of infrastructure challenges: assessing stormwater system sustainability. Can. J. Civ. Eng. 41 (6), 483–492. https://doi.org/10.1139/cjce-2013-0430.
Villarini, G., Smith, J.A., Baeck, M.L., Krajewski, W.F., 2011. Examining flood frequency distributions in the Midwest U.S.1. JAWRA. J. Am. Water Resour. Assoc. 47 (3), 447–463. https://doi.org/10.1111/j.1752-1688.2011.00540.x.
Vu, C.H., Nguyen, B.Q., Tran, T.-N.-D., Vo, D.N., Arshad, A., 2024. Climate change-driven hydrological shifts in the Kon-ha Thanh River basin. Water 16 (23), 3389. https://doi.org/10.3390/w16233389.
Wahl, T., Jain, S., Bender, J., Meyers, S.D., Luther, M.E., 2015. Increasing risk of compound flooding from storm surge and rainfall for major US cities. Nat. Clim. Chang. 5 (12), 1093–1097. https://doi.org/10.1038/nclimate2736.
Walsh, C.J., Booth, D.B., Burns, M.J., Fletcher, T.D., Hale, R.L., Hoang, L.N., Livingston, G., Rippy, M.A., Roy, A.H., Scoggins, M., Wallace, A., 2016. Principles for urban stormwater management to protect stream ecosystems. Freshw. Sci. 35 (1), 398–411. https://doi.org/10.1086/685284.
Wang, P., Li, Y., Yu, P., Zhang, Y., 2021. The analysis of urban flood risk propagation based on the modified susceptible infected recovered model. J. Hydrol. 603, 127121. https://doi.org/10.1016/j.jhydrol.2021.127121.
Wang, X., Kinsland, G., Poudel, D., Fenech, A., 2019. Urban flood prediction under heavy precipitation. J. Hydrol. 577, 123984. https://doi.org/10.1016/j.jhydrol.2019.123984.
Weber, A., 2019. What Is Urban Flooding? https://www.nrdc.org/bio/anna-weber/what-urban-flooding. (Accessed 24 April 2024).
Wu, X., Wang, Z., Guo, S., Liao, W., Zeng, Z., Chen, X., 2017. Scenario-based projections of future urban inundation within a coupled hydrodynamic model framework: a case study in Dongguan City, China. J. Hydrol. 547, 428–442. https://doi.org/10.1016/j.jhydrol.2017.02.020.
Xu, K., Ma, C., Lian, J., Bin, L., 2014. Joint probability analysis of extreme precipitation and storm tide in a coastal city under changing environment. PLoS One 9 (10), e109341. https://doi.org/10.1371/journal.pone.0109341.
Yan, L., Rong, H., Yang, W., Lin, J., Zheng, C., 2024. A novel integrated urban flood risk assessment approach based on one-two dimensional coupled hydrodynamic model and improved projection pursuit method. J. Environ. Manag. 366, 121910. https://doi.org/10.1016/j.jenvman.2024.121910.
Yazdanfar, Z., Sharma, A., 2015. Urban drainage system planning and design–challenges with climate change and urbanization: a review. Water Sci. Technol. 72 (2), 165–179. https://doi.org/10.2166/wst.2015.207.
Ye, C., Xu, Z., Lei, X., Zhang, R., Chu, Q., Li, P., Ban, C., 2022. Assessment of the impact of urban water system scheduling on urban flooding by using coupled hydrological and hydrodynamic model in Fuzhou City, China. J. Environ. Manag. 321, 115935. https://doi.org/10.1016/j.jenvman.2022.115935.
Yin, J., Lin, N., Yu, D., 2016a. Coupled modeling of storm surge and coastal inundation: a case study in new York City during hurricane Sandy. Water Resour. Res. 52 (11), 8685–8699. https://doi.org/10.1002/2016WR019102.
Yin, J., Yu, D., Yin, Z., Liu, M., He, Q., 2016b. Evaluating the impact and risk of pluvial flash flood on intra-urban road network: a case study in the city center of Shanghai, China. J. Hydrol. 537, 138–145. https://doi.org/10.1016/j.jhydrol.2016.03.037.
Zandsalimi, Z., Feizabadi, S., Yazdi, J., Salehi Neyshabouri, S.A.A., 2024. Evaluating the impact of digital elevation models on urban flood modeling: a comprehensive analysis of flood inundation, hazard mapping, and damage estimation. Water Resour. Manag. https://doi.org/10.1007/s11269-024-03862-4.